

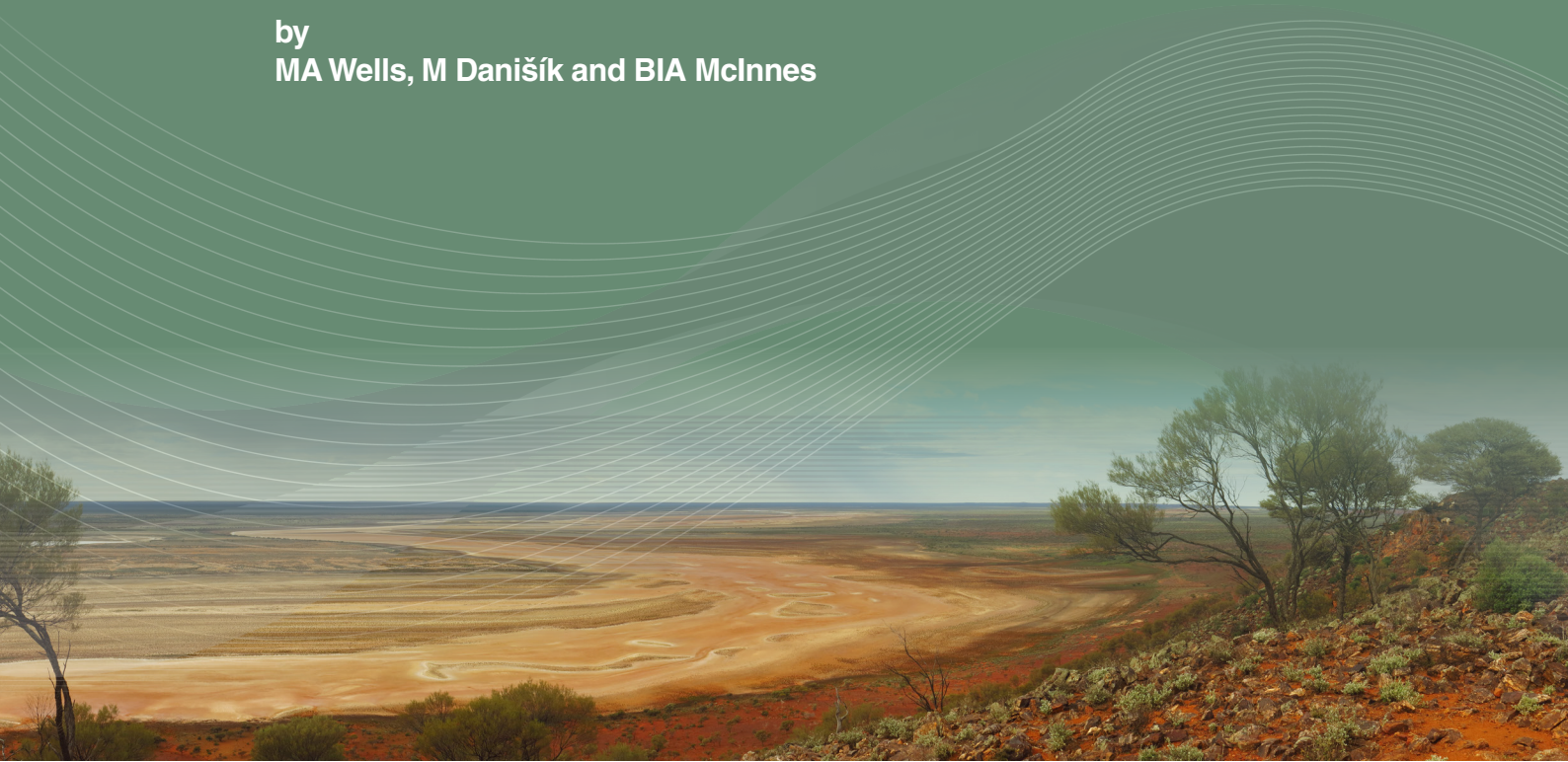


Government of **Western Australia**
Department of **Mines, Industry Regulation and Safety**

RECORD 2018/13

(U–TH)/HE DATING OF FERRUGINOUS DURICRUST, BODDINGTON GOLD MINE, WESTERN AUSTRALIA

by
MA Wells, M Danišík and BIA McInnes



Geological Survey of Western Australia



Government of **Western Australia**
Department of **Mines, Industry Regulation and Safety**

RECORD 2018/13

(U–TH)/HE DATING OF FERRUGINOUS DURICRUST, BODDINGTON GOLD MINE, WESTERN AUSTRALIA

by
MA Wells*, M Danišík* and BIA McInnes*

* John de Laeter Centre, Curtin University, GPO Box U1987, Perth WA 6845

PERTH 2018



**Geological Survey of
Western Australia**

MINISTER FOR MINES AND PETROLEUM
Hon Bill Johnston MLA

DIRECTOR GENERAL, DEPARTMENT OF MINES, INDUSTRY REGULATION AND SAFETY
David Smith

DIRECTOR, GEOSCIENCE AND RESOURCE STRATEGY
Jeff Haworth

REFERENCE

The recommended reference for this publication is:

Wells MA, Danišik M and McInnes BIA 2018, (U–Th)/He dating of ferruginous duricrust, Boddington gold mine, Western Australia: Geological Survey of Western Australia, Record 2018/13, 14p.

ISBN 978-1-74168-833-7

ISSN 0728-2311

Grid references in this publication refer to the Geocentric Datum of Australia 1994 (GDA94). Locations mentioned in the text are referenced using Map Grid Australia (MGA) coordinates, Zone 50. All locations are quoted to at least the nearest 100 m.

Disclaimer

This product was produced using information from various sources. The Department of Mines, Industry Regulation and Safety (DMIRS) and the State cannot guarantee the accuracy, currency or completeness of the information. Neither the department nor the State of Western Australia nor any employee or agent of the department shall be responsible or liable for any loss, damage or injury arising from the use of or reliance on any information, data or advice (including incomplete, out of date, incorrect, inaccurate or misleading information, data or advice) expressed or implied in, or coming from, this publication or incorporated into it by reference, by any person whosoever.

 John de Laeter Centre

 EXPLORATION
INCENTIVE
SCHEME

(U–Th)/Pb measurements were conducted at the John de Laeter Centre, Curtin University.

Published 2018 by the Geological Survey of Western Australia

This Record is published in digital format (PDF) and is available online at <www.dmp.wa.gov.au/GSWApublications>.



© State of Western Australia (Department of Mines, Industry Regulation and Safety) 2018

With the exception of the Western Australian Coat of Arms and other logos, and where otherwise noted, these data are provided under a Creative Commons Attribution 4.0 International Licence. (<http://creativecommons.org/licenses/by/4.0/legalcode>)

Further details of geological products and maps produced by the Geological Survey of Western Australia are available from:

Information Centre
Department of Mines, Industry Regulation and Safety
100 Plain Street
EAST PERTH WESTERN AUSTRALIA 6004
Telephone: +61 8 9222 3459 Facsimile: +61 8 9222 3444
www.dmp.wa.gov.au/GSWApublications

Cover image: Elongate salt lake on the Yilgarn Craton — part of the Moore–Monger paleovalley — here viewed from the top of Wownamina Hill, 20 km southeast of Yalgoo, Murchison Goldfields. Photograph by I Zibra, DMIRS

Contents

Abstract	1
Introduction	1
Methodology	3
Samples	3
Mineralogy and geochemical characterization.....	3
Geochronology.....	3
Results.....	4
Geochemistry and mineralogy	4
Raman analysis	4
(U–Th)/He geochronology	6
Discussion	10
Conclusions	10
Acknowledgements	10
References	11

Figures

1. Field locality of the Boddington gold mine (BGM) and locations of regolith samples.....	2
2. Polished mount and reflected light photomicrographs of sample GSWA 226923	6
3. Backscattered electron (BSE) images and false-colour TIMA mineral distribution maps of samples of pisolitic and fragmental duricrust	7
4. Polished mount of pisolitic duricrust (GSWA 226971), and optical micrographs and Raman spectra of two pisolites	8
5. U + Th content vs radiogenic He volume for BGM duricrust samples.....	9
6. Ranked order plot of (U–Th)/He dates for BGM duricrust samples.....	9
7. Radial plot of (U–Th)/He dates for sample GSWA 226923.....	9
8. X-ray diffraction (XRD) patterns for the pisolite rim and core in GSWA 226923	11

Tables

1. Location and description of regolith samples collected at BGM.....	3
2. Bulk geochemical composition of BGM duricrust samples.....	4
3. Random powder bulk XRD mineralogy of BGM pisolitic and fragmental duricrust	5
4. Raman bands of phases detected in BGM duricrust compared to well-characterized hematite, maghemite, goethite and gibbsite.....	5
5. Corrected (U–Th)/He dates and Th/U ratios for BGM duricrust (cored pisolites) and for pisolitic duricrust near Toodyay	7

Appendix

Raw and corrected (U–Th)/He dates and measured U, Th and He concentrations for analysed duricrust samples	12
--	----

(U–Th)/He dating of ferruginous duricrust, Boddington gold mine, Western Australia

by

MA Wells*, M Danišík* and BIA McInnes*

Abstract

Ferruginous duricrust from exposed laterite profiles near the Boddington gold mine (BGM) were sampled and assessed for their suitability for (U–Th)/He dating. Optical microscopy, Raman spectroscopy, XRD analysis, and Tescan Integrated Mineral Analyzer (TIMA) mineral mapping confirms the suitability of pisolitic duricrust (pisolites and nodules) for (U–Th)/He dating as well as showing that the duricrust matrix and pisolite cutans are too porous and mineralogically heterogeneous for dating purposes. (U–Th)/He dates of 5.7 – 1.3 Ma for pisolitic and fragmental duricrust indicate late Miocene–Pliocene to possible early Pleistocene ages for the formation of pisolites and nodules in BGM duricrust. These results are comparable with (U–Th)/He data for pisolitic duricrust near Toodyay, and are consistent with other age estimates for lateritization in Western Australia, suggesting that processes of regolith formation and/or modification in the Darling Range were regionally synchronous. The significant difference in age of the rim (2.0 ± 0.2 Ma) compared to the core (3.9 ± 0.5 Ma) of a single pisolite, in conjunction with a difference in mineralogy, suggests that ancient episodic bushfires may have affected or reset (U–Th)/He ages of iron oxides. Despite this, the isotopic technique remains useful in providing quantitative constraints on the minimum age of regolith formation.

KEYWORDS: Boddington, Darling Range, duricrust, iron oxides, Miocene, Pliocene, regolith, (U–Th)/He dating

Introduction

The Boddington gold mine (BGM), located on the Darling Range, 130 km southeast of Perth, is one of the largest gold mines in Australia (Fig. 1). The deposit is hosted by 2717–2690 Ma intrusive and volcanic rocks (diorite and andesite) of the Saddleback greenstone belt in the southwest Yilgarn Craton (McCuaig et al., 2001). Weathering of the Archean host rocks has resulted in the development of a thick regolith profile throughout the Darling Range area (Anand and Butt, 2003).

At the BGM, the regolith comprises clay-rich saprolite (25–70 m thick), overlain by a gibbsite-rich bauxite zone (about 4 m thick) and ferruginous duricrust (1.5 – 3.0 m thick). Throughout the Darling Range, this material comprises a lower zone of fragmental duricrust overlain by an upper zone of pisolitic material, although a transitional zone can also be locally developed (Anand, 2005). Fragmental duricrust contains red (hematite-rich) to dark brown, subangular to angular fragments up to 30 mm in size (Anand and Butt, 2003; Anand, 2005). Pisolitic duricrust is more Fe rich and contains red to almost black, well-rounded, simple or compound nodules and pisolites, ranging from about 5 to 20 mm in diameter, that contain a high proportion of hematite and maghemite (Anand and Butt, 2003). Fragmental duricrust is regarded as largely

residual due to the presence of clasts that preserve the primary fabric of the granite bedrock, whereas textural evidence indicates the pisolitic duricrust is residual or locally transported (Anand and Butt, 2003; Anand, 2005).

Despite its prevalence in the Australian landscape, there is a significant gap in our knowledge of the timescales of regolith formation. The geochronology of weathered materials has been investigated by paleomagnetic and K–Ar and Ar/Ar techniques on a limited scale (see review by Pillans, 2005). The paleomagnetic method is an indirect approach, and Ar techniques are limited by suitability of appropriate K-bearing minerals in the regolith. The efforts of Wernicke and Lippolt (1994) to revive the (U–Th)/He technique pioneered by Fanale and Kulp (1962) on Fe-oxides, combined with new infrastructure investments enabling the (U–Th)/He measurements at Curtin University’s John de Laeter Centre in 2004, has provided a new isotopic tool for quantitatively understanding regolith histories. The application of (U–Th)/He dating in Western Australia includes an initial study by Pidgeon et al. (2004) of Darling Range pisolitic duricrust from the Toodyay area which yielded dates of 10.0 – 7.5 Ma. Complementary geochronological studies of the economically important Pilbara channel iron deposits (CID) reported dates ranging from 25.7 to 6.0 Ma (Heim et al., 2006; Danišík et al., 2013; Vasconcelos et al., 2013). Hence, the (U–Th)/He dating method is becoming established as a suitable technique for chronological studies in the formation of low-temperature ferruginous materials.

* John de Laeter Centre, Curtin University, GPO Box U1987, Perth WA 6845

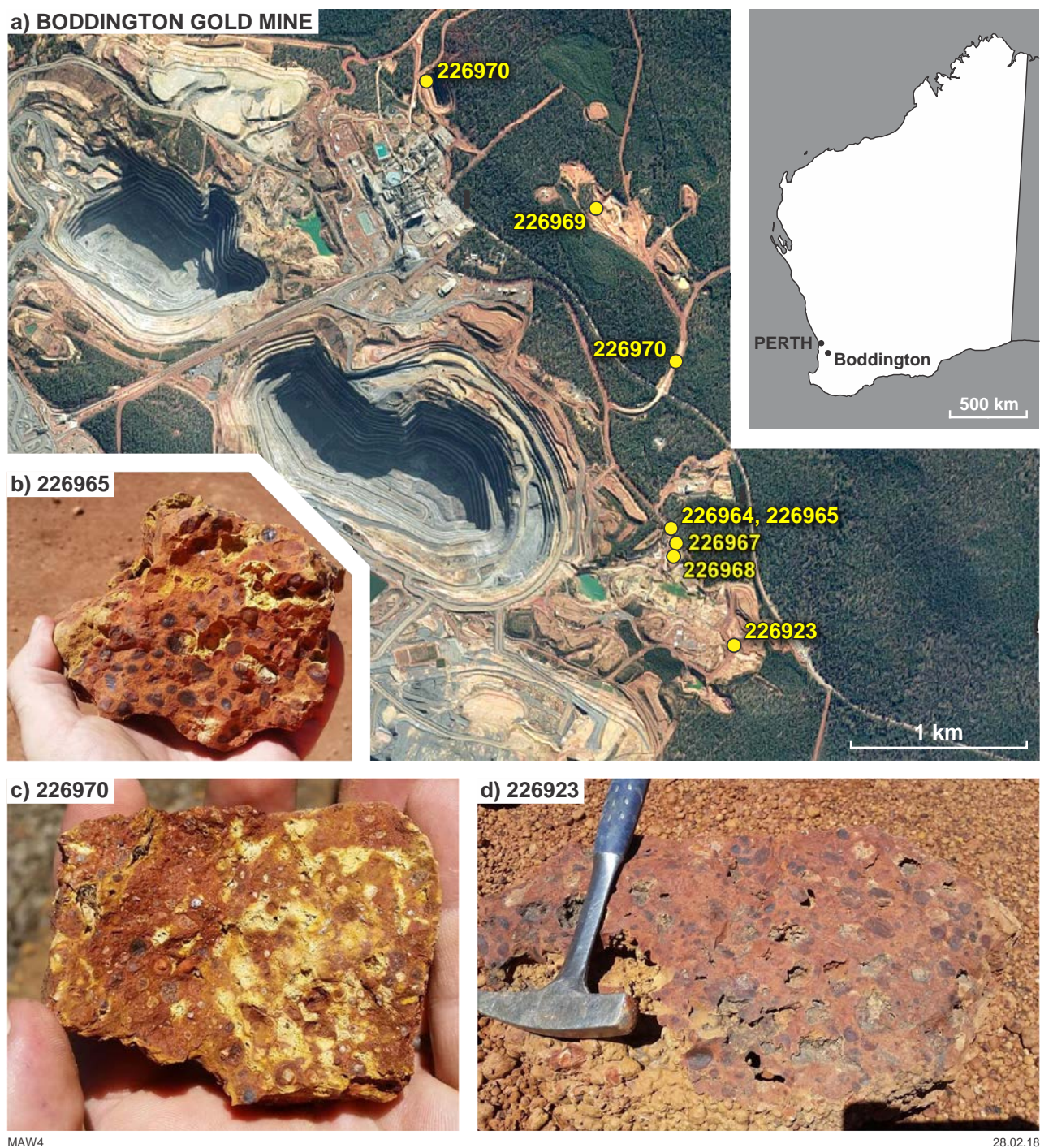


Figure 1. Location information: a) field locality of the Boddington gold mine (BGM) and locations of regolith samples collected for (U–Th)/He dating; b–d) field photos of representative examples of pisolitic (GSWA 226923, 226965) and fragmental (GSWA 226970) duricrust. Photos by Paul Morris, GSWA

This study was undertaken to assess the type of duricrust material (e.g. fragmental vs pisolitic) most suitable for application of the (U–Th)/He dating technique by systematically collecting samples from exposures in the BGM, characterizing these materials by microscopy and isotopic techniques, and comparing the results with those obtained by Pidgeon et al. (2004). It was anticipated at the onset of the project that the combined results would provide a quantitative temporal framework for understanding landscape evolution and regolith formation in the Darling Range.

Methodology

Samples

Samples of fragmental and pisolitic duricrust, as defined by Anand and Butt (2003), were collected from regolith profiles exposed at the BGM (Fig. 1) with field descriptions and location coordinates listed in Table 1.

Mineralogy and geochemical characterization

Bulk mineralogical and geochemical characterization, followed by optical microscopy, Raman spectroscopy and automated mineral mapping using a TESCAN Integrated Mineral Analyser (TIMA) were used to identify areas within samples and material types (e.g. matrix, cutans or pisolites) most suited for (U–Th)/He dating. Whole-rock geochemical analysis (26 elements) was conducted using X-ray fluorescence spectroscopy of fused glass disks by Bureau Veritas Minerals Pty Ltd. Uranium and Th were measured separately using laser ablation inductively coupled mass spectrometry (LA-ICPMS). Loss on ignition (LOI) at 1000°C was determined using a robotic Thermogravimetric Analysis (TGA) system. Bulk

powder X-ray diffraction (XRD) analysis for identification of mineral phases was conducted using a Bruker D8 Discover diffractometer using CoK α radiation with mineral identification facilitated using the Bruker DIFFRAC.EVA V3.2 software at Curtin University.

For each duricrust sample, two polished epoxy mounts (25 mm diameter) were prepared, with one used for in situ mineralogical characterization using optical microscopy and Raman spectroscopy, and the other for TIMA mineral mapping. For Raman analysis, a WITec Alpha 300SAR (S = Scanning Near Field Optical Microscope, A = Atomic Force Microscope, R = Raman) instrument was used operating a frequency-doubled Nd YAG laser at an excitation wavelength of 532 nm and maximum power output of 50 mW. Typically, Raman spectra were collected using a Zeiss 20x/0.4NA microscope objective. Combined mineral and elemental mapping used the TIMA energy dispersive spectrography system with mapping of selected areas at a spatial resolution of 7 μ m.

Geochronology

Regions of interest (ROIs) within nodules and pisolites identified as suitable for (U–Th)/He dating were sampled by mini-coring using a diamond drill to extract a core about 3 mm in diameter and 3–5 mm in length. Cores from two pisolites for each duricrust sample were crushed and sieved to recover 200–300 μ m size shards. No suitable area in GSWA 226970 was identified for coring due to the high degree of sample inhomogeneity. Instead, a hematite–goethite rich, lithic fragment was selected for (U–Th)/He dating. Five replicates of each crushed core or lithic material were prepared by loading ultrasonically cleaned shards, selected under an optical microscope, into Nb microtubes. Details of the (U–Th)/He dating method used are described by Danišák et al. (2013). In summary, He analysis involved laser extraction and noble gas mass spectrometry, followed by spiking with ^{230}Th and ^{235}U , dissolution in HCl, and U–Th measurement by isotope dilution ICPMS.

Table 1. Location and description of regolith samples collected at BGM

GSWA sample ID	Zone	Easting (m)	Northing (m)	Elevation (m ASL)	Sample type	Notes
226923	50	441774	6374759	260	Pisolitic duricrust	Matrix supported, 0.3 – 1 cm pisolites (some concentric), slightly magnetic
226965	50	441407	6375482	299	Pisolitic duricrust	Top of profile; 3 m thick layer
226969A,B*	50	440959	6377253	341	Fragmental duricrust	From Pit K4; nonmagnetic to slightly magnetic; aluminous
226970	50	441418	6376361	320	Fragmental duricrust	Roadside sample; quartz grains from underlying granite; gypsum and boehmite (bauxite minerals) fill pores; formed in depositional environment
226971A,B*	50	440004	6377924	319	Pisolitic duricrust	From Q pit; Fe-rich, porous, quartz crystals in matrix; very magnetic

NOTE: *Sample consists of two parts, denoted A and B. Coordinates in MGA94. Abbreviations: ASL, above sea level

Results

Geochemistry and mineralogy

Whole-rock geochemistry (Table 2) is similar to data previously reported for Darling Range laterite by Anand and Butt (2003). Weight percent SiO_2 , Al_2O_3 , Fe_2O_3 and TiO_2 contents, together with LOI values, account for >99 wt% of the total duricrust composition. Sample GSWA 226970 is notable for its high Th (1220 ppm), U (11.4 ppm), and Zr (0.12%) contents, suggesting that zircon may be present in this sample.

The bulk mineralogy (Table 3) is consistent with previous studies of laterite in the Darling Range area and the mineralogical differences reported between fragmental and pisolitic duricrust (Anand and Butt, 2003). Typically, duricrust mineralogy is dominated by gibbsite and Fe-oxides (hematite, maghemite, goethite), with gibbsite commonly present in significant amounts in fragmental duricrust (and bauxite), but less common in pisolitic duricrust (Anand and Butt, 2003). Quartz is ubiquitous and represents a relict phase, the abundance of which depends on the parent rock from which it was sourced (e.g. granitic vs mafic volcanic; Anand and Butt, 2003). Similarly, muscovite (e.g. GSWA 226965, Table 3) also represents a relict phase from granitic rocks and is typically present in low amounts (<1–3 wt%). The identification of maghemite (e.g. GSWA 226923, Table 3) and, particularly, corundum (GSWA 226971B, Table 3) may have implications for duricrust genesis, and is discussed further in relation to the (U–Th)/He dating results.

Optical microscopic examination of polished epoxy mounts (Fig. 2) highlights the heterogeneous and porous nature of the cementing matrix in the duricrust, of cutans on the margins of pisolites, and of nodules in the duricrust (Fig. 2). To minimize the potential loss or gain of radiogenic ^4He , the ideal material for (U–Th)/He dating is near monomineralic, texturally uniform, with low porosity and showing little evidence of leaching (Pidgeon et al., 2004). Mineral distribution mapping shows that the nodular or pisolitic components of duricrust are the least mineralogically complex and most texturally uniform with little or no evidence of leaching compared to either the duricrust matrix or cutan material (e.g. sample GSWA 226923, Fig. 3). Hence, further mineralogical characterization using Raman analysis focused on confirmation of the pisolite mineralogy.

Raman analysis

Wavenumber positions of minerals identified using Raman analysis in ROIs in pisolites targeted for (U–Th)/He dating are listed in Table 4, with representative Raman spectra of two pisolites in sample GSWA 226971A shown in Fig. 4. The Raman bands detected are matched against known Raman band wavenumbers for standard or well-characterized hematite, maghemite, goethite, and gibbsite (Ramanaidou et al., 2015). This confirms that pisolite mineralogy consists mainly of hematite and maghemite (Table 4).

Table 2. Bulk geochemical composition of BGM duricrust samples

GSWA sample ID	SiO_2 (%)	Fe_2O_3 (%)	Al_2O_3 (%)	TiO_2 (%)	MnO (%)	CaO (%)	SO_3 (%)	MgO (%)	K_2O (%)	V_2O_5 (%)	Th (ppm)	U (ppm)	LOI 371 (%)	LOI 371–650 (%)	LOI 650–1000 (%)	LOI 1000 (%)	Total oxides (%)
226923	0.67	39.8	39.9	2.95	0.005	0.01	0.16	-0.01	0.01	0.140	15.7	2.77	14.0	1.85	0.57	16.4	100.0
226965	1.94	22.1	47.6	2.14	-0.001	0.01	0.15	-0.01	0.108	0.081	65.1	6.18	22.0	3.18	0.84	26.0	100.1
226969A	1.06	37.1	36.4	2.34	0.026	0.01	0.27	-0.01	0.013	0.134	12.4	2.88	19.5	2.46	0.82	22.7	100.1
226969B	1.06	41.7	33.5	1.92	0.020	0.01	0.28	-0.01	0.006	0.167	11.7	2.74	17.8	2.50	0.81	21.1	99.7
226970	25.6	25.0	30.2	0.50	0.004	0.01	0.17	0.01	0.227	0.038	1220	11.4	14.9	2.37	0.62	17.8	99.6
226971A	0.59	74.1	14.6	3.04	0.011	0.01	0.27	0.01	0.003	0.299	6.55	1.73	5.98	0.71	0.53	7.22	100.1
226971B	0.55	76.0	12.6	3.42	0.009	0.01	0.25	0.01	0.002	0.305	5.53	1.34	5.70	0.69	0.52	6.90	100.1

NOTE: Element abundances: P (<0.04%), Cu and Ba (<0.03%), Cr (<0.08%), Cl (<0.03%), As, Ni, Co, Sn and Sr (<0.01%); Zr (<0.06%, except GSWA 226970), Zn and Pb are below detection limit

Table 3. Random powder bulk XRD mineralogy of BGM pisolitic and fragmental duricrust

<i>GSWA sample ID</i>	<i>Sample type</i>	<i>Mineralogy*</i>
226923	Pisolitic duricrust	Gibbsite, maghemite, hematite (maj); anatase, goethite, quartz (tr)
226965	Pisolitic duricrust	Gibbsite (maj); hematite, goethite (min); anatase, quartz, muscovite (tr)
226969A	Fragmental duricrust	Gibbsite (maj); goethite, hematite (min); anatase (tr)
226969B	Fragmental duricrust	Gibbsite (maj); goethite, hematite (min); anatase, quartz (tr)
226970	Fragmental duricrust	Quartz, gibbsite (maj); goethite, hematite (min); kaolinite, muscovite (tr)
226971A	Pisolitic duricrust	Hematite, goethite (maj); gibbsite, maghemite (min); corundum, quartz, anatase (tr)
226971B	Pisolitic duricrust	Hematite, goethite (maj); gibbsite, maghemite, corundum? (min); quartz, anatase, rutile? (tr)

NOTE: *Mineral abundances are qualitatively listed as occurring in major (maj), minor (min) and trace (tr) amounts

Table 4. Raman bands of phases detected in BGM duricrust compared to well-characterized hematite, maghemite, goethite and gibbsite

<i>GSWA sample ID</i>	<i>ROI</i>	<i>Raman bands (cm⁻¹)</i>							
226923	ROI4_Rim	226	292	405	508	614	669	1331	
226923	ROI4_Core	218	281	386					
226965	ROI2		299	410			671	1337	
226965	ROI3	229	298	415	509		673	1333	
226969	R1B		247	320	386	542	569	897	
226971	ROI2	224	291	405	498	608		1320	
226971	ROI3	227	295	411	505	617	670	1335	
<i>Standards</i>									
Hematite*		223–228	296–302	406–423	496–501	611–618			
Maghemite*			263–265	292–295	345–350	380–395	505–515	645–665	715–740
Goethite*			243–247	298–308	385–399	470–486	547–560	679–685	
Gibbsite^			242	321		539	568	892	

NOTE: Raman bands for mineral standards highlighted in bold are the most diagnostic bands detected for each phase. These are colour coded where the band was detected in each duricrust sample. * Ramanaidou et al. (2015); ^ Ruan et al. (2001)

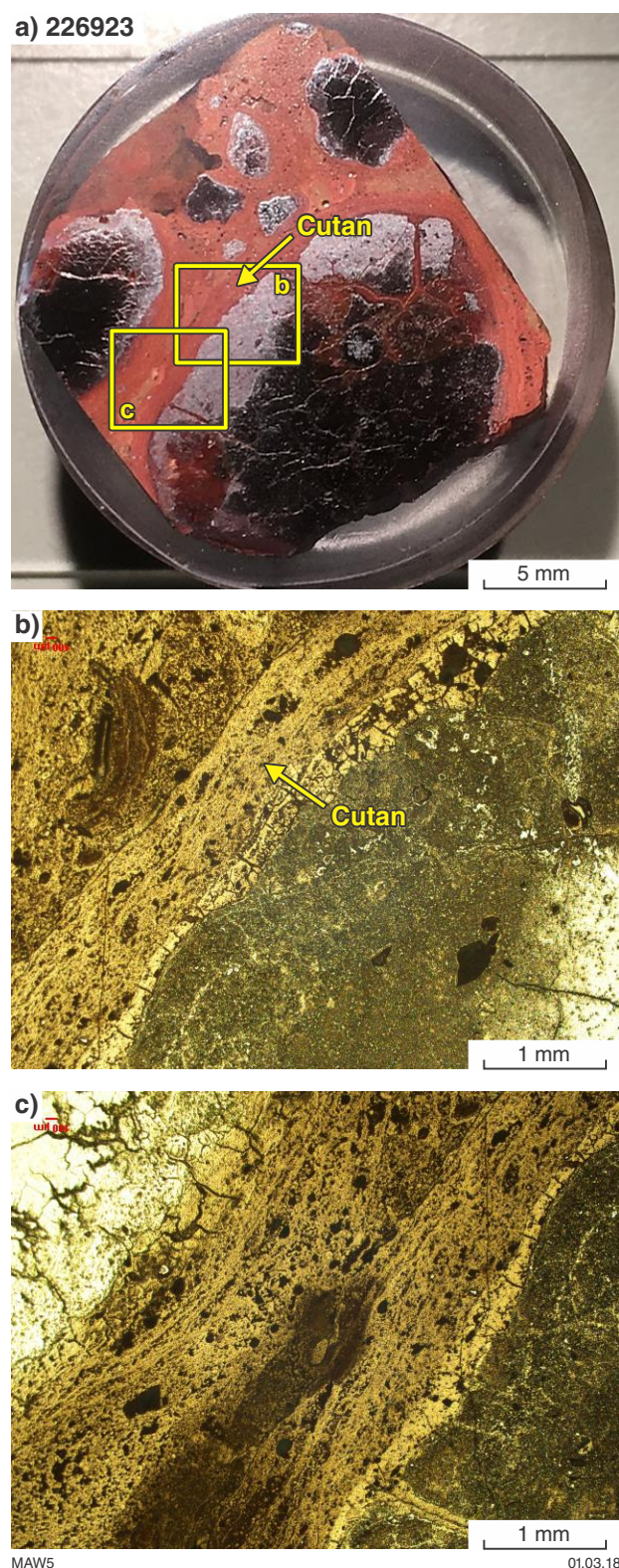


Figure 2. Polished mount and reflected light photomicrographs of sample GSWA 226923 (pisolitic duricrust)

(U–Th)/He geochronology

Final (U–Th)/He ages for all ROIs, together with measured U, Th, and He contents, are tabulated in the Appendix. A summary of the final, averaged (U–Th)/He dates is provided in Table 5, with the results indicating a late Miocene–Pliocene to possible early Pleistocene age for the BGM duricrust. These ages are consistent with the (U–Th)/He dates of 10.0 – 7.5 Ma obtained for pisolitic and fragmental duricrust from Morangup Hill, in the Darling Range near Toodyay (Pidgeon et al., 2004). Measured Th/U ratios for BGM duricrust are also similar to those in the Toodyay duricrust (Table 5), which were interpreted to indicate that the measured Th/U ratios had remained fixed since formation of the duricrust (Pidgeon et al., 2004). The exception is the very high Th/U ratio of 448.4 for the mottle in sample GSWA 226970 due mainly to the very high Th content (Table 2), mainly present in zircon and possibly thorianite (ThO_2) detected in the TIMA mineral maps. The source of thorianite is unknown.

A potential source of error associated with (U–Th)/He dating is the loss of ^4He and loss or gain of uranium and/or thorium (Pidgeon et al., 2004). The strong correlation between the measured U–Th content and evolved volume of He (Fig. 5) suggests that the pisolites in BGM duricrust represent a closed system and have not been affected by postformation processes that could have resulted in a net loss of He.

The distribution of averaged (U–Th)/He dates for selected duricrust samples shows there is no local trend or distribution at BGM. A ranked order plot of the (U–Th)/He dates for BGM duricrust better demonstrates the relative age differences between individual duricrust samples and the range in the (U–Th)/He dates measured in each case (Fig. 6). It is interesting to note a possible difference in the (U–Th)/He dates between the rim (2.0 ± 0.2 Ma) and core (3.8 ± 0.5 Ma) for sample GSWA 226923 (Fig. 6). This is examined more closely in a radial plot of the (U–Th)/He dates (Fig. 7).

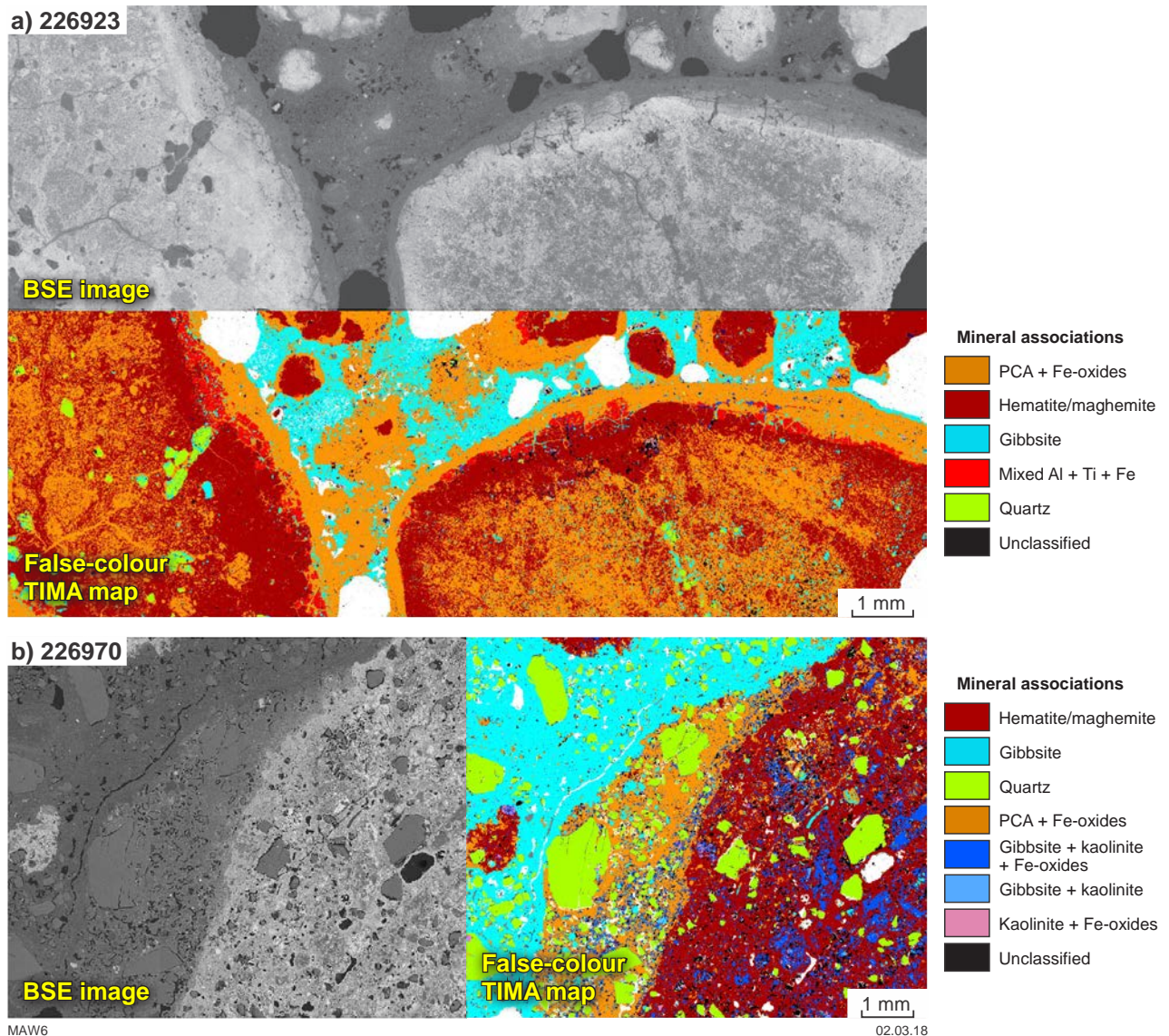
Deconvolution of (U–Th)/He dates using ‘Mixture Models’ function in RadialPlotter software (Vermeesch, 2009) provides a means of identifying principal components in the measured duricrust (U–Th)/He dates. A radial plot of the (U–Th)/He dates measured for the pisolite rim and core in GSWA 226923 suggests the pisolite rim is significantly younger than the pisolite core (Fig. 7). The dated rim sample has a higher Th/U ratio (nearly double) compared to the Th/U ratio measured for the dated pisolite core (refer to Table 5 and the Appendix). The measured Th contents for the rim and core are similar, with measured U contents supporting some loss of U from the pisolite rim.

Figure 3. (page 7) Backscattered electron (BSE) images and false-colour TIMA mineral distribution maps for samples of: a) pisolitic duricrust (GSWA 226923) and; b) fragmental duricrust (GSWA 226970). Mineral mapping better highlights the complexity of the mineralogical associations and compositional variations for each sample than can be observed using either optical or BSE imagery. Pisolites and nodules are more representative of a closed, mineralogically and texturally uniform system at the scale of sampling required for (U–Th)/He dating compared to other components (matrix, cutans) of the duricrust

Table 5. Corrected (U–Th)/He dates and Th/U ratios for BGM duricrust (cored pisolites) and for pisolitic duricrust near Toodyay

GSWA sample ID	Region of interest (ROI)	Corrected He date (Ma)	$\pm 1\sigma$ (Ma)	Th/U	Elevation (m ASL)
226971	R1A_roi2-1	5.7	0.7	9.65	319
226971	R1A_roi3-1	3.8	0.5	4.92	319
226971	R1B_roi4-1	5.8	0.7	7.35	319
226971	R1B_roi5-1	3.8	0.5	8.13	319
226965	R2_roi2-1	5.2	0.6	13.30	299
226965	R2_roi3-1	3.2	0.4	12.85	299
226923	R3_roi2-1	2.3	0.3	5.32	260
226923	R3_roi4-1 rim	2.0	0.2	15.14	260
226923	R3_roi4-1 core	3.8	0.5	8.50	260
226969	R1B_roi1-1	2.9	0.8	2.81	341
226970	MottleDat-1	1.3	0.1	448.35	320
<i>Toodyay samples (Pidgeon et al., 2004)</i>					
Sa1		9.9	0.6	8 (± 0.3)	
Sa2		7.5	0.6	17.4 (± 0.6)	
Sa3		9.1	1.8	7.6 (± 0.3)	
Sa7		10	0.7	15.3 (± 0.5)	

NOTE: Abbreviation: ASL, above sea level



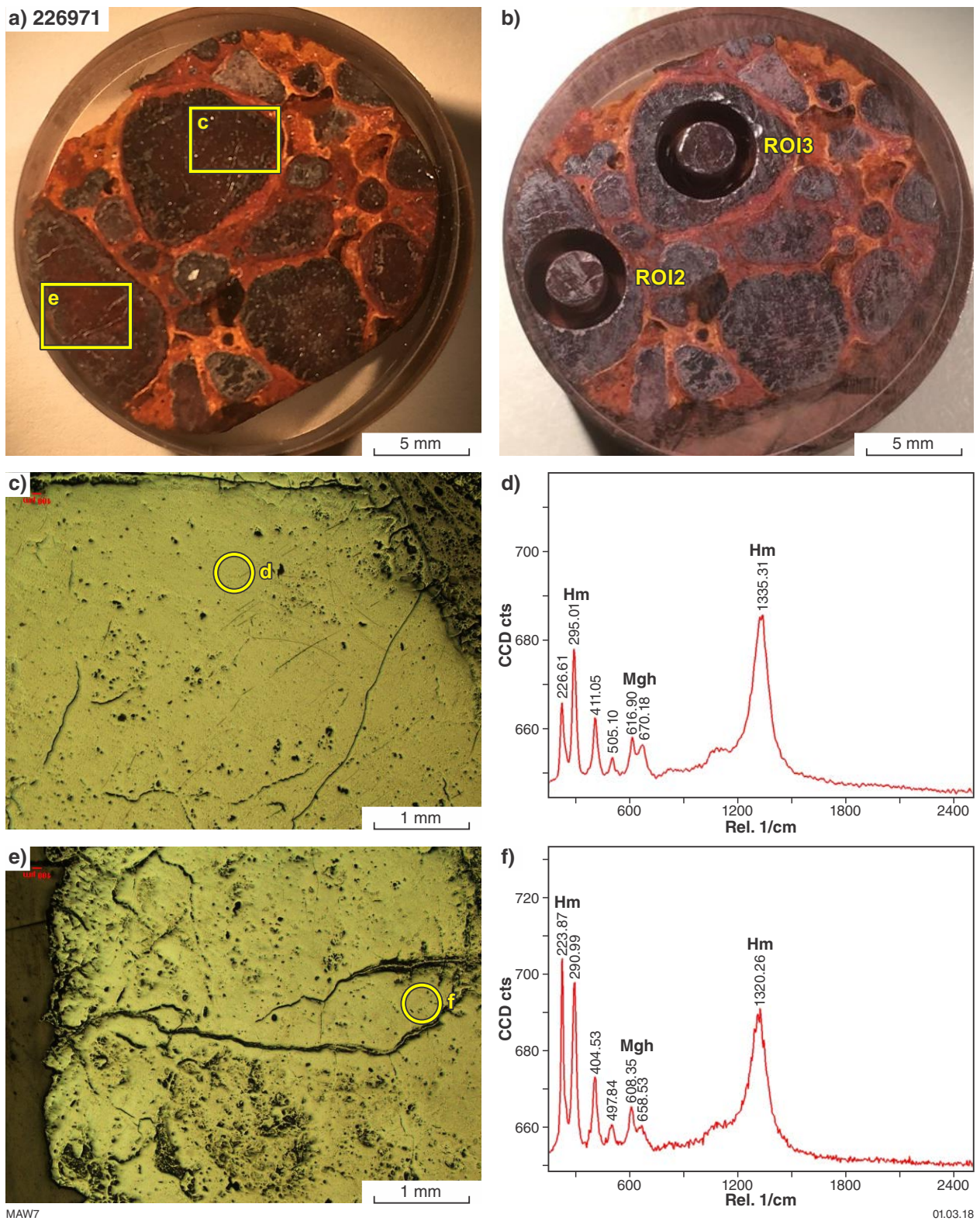


Figure 4. Polished mount of pisolitic duricrust in sample GSWA 226971: a) locations of ROIs (c, e) identified in pisolites prior to being cored for (U–Th)/He dating (b); c, e) optical micrographs of the two ROIs outlined in (a); d, f) Raman spectra at locations within each pisolite, as shown by the circles in the optical micrographs (c, e), enable in situ identification of pisolite mineralogy. Peaks in the Raman spectra confirm the presence of maghemite (Mgh) and hematite (Hm)

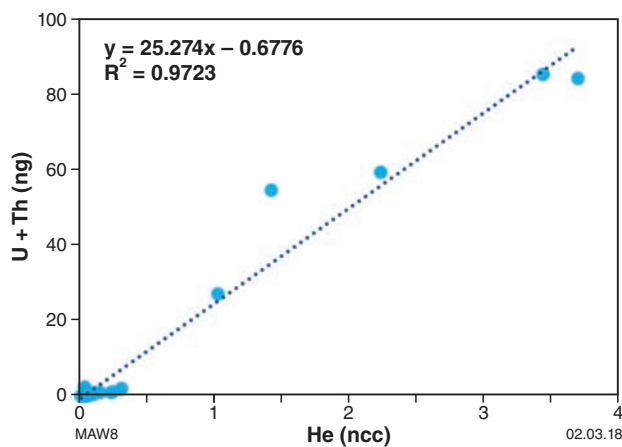


Figure 5. U + Th content vs radiogenic He volume for BGM duricrust samples. The strong correlation indicates that there has not been a significant loss or gain of He. Abbreviations: ng, nanogram; ncc, nano cubic centimetres

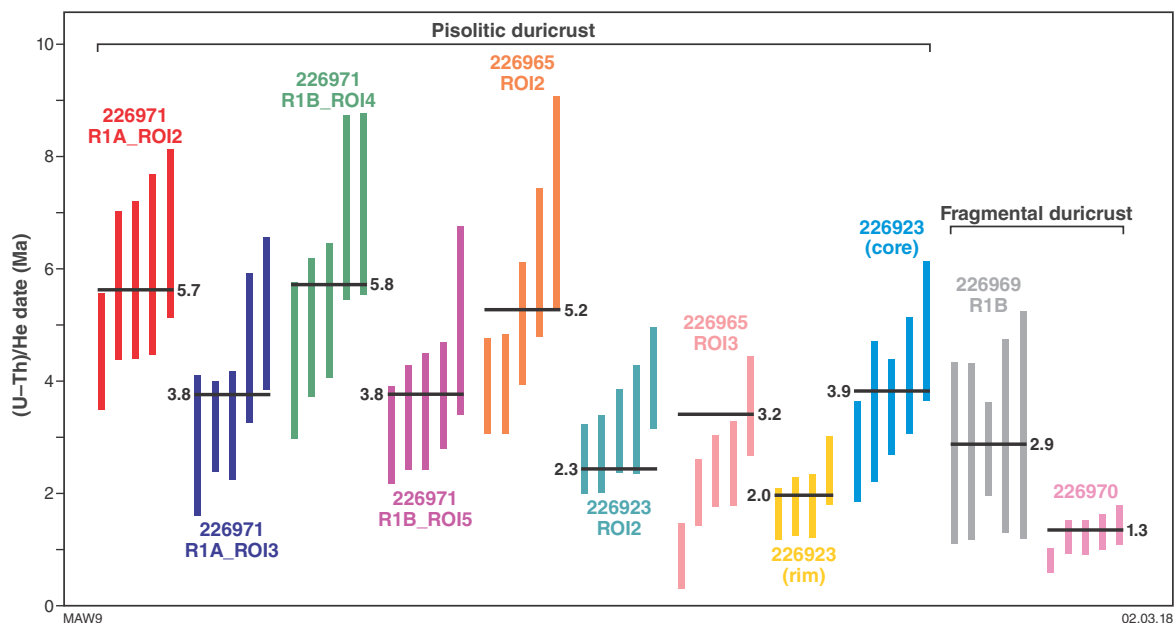


Figure 6. Ranked order plot of (U–Th)/He dates for BGM duricrust samples. Coloured bars represent individual replicate measurements with the length of each bar indicating the 1σ uncertainty. The black horizontal bars indicate the average (U–Th)/He age (in Ma) assigned to each duricrust sample

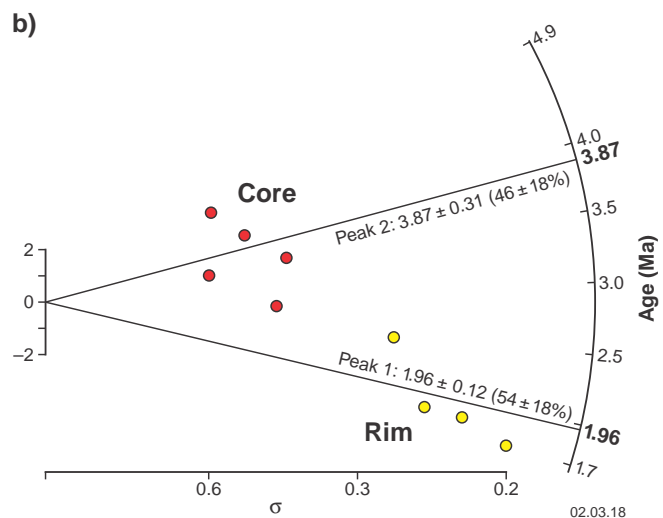
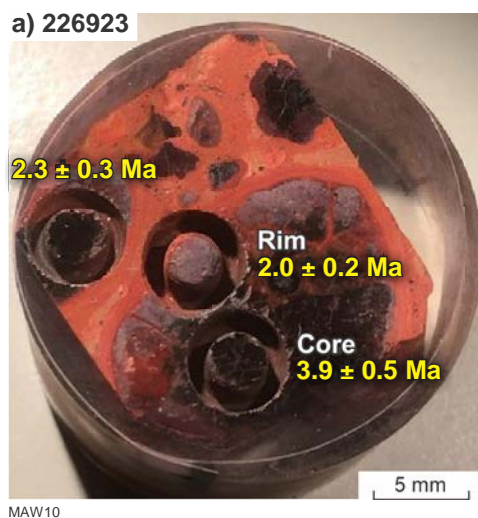


Figure 7. (U–Th)/He results for sample GSWA 226923: a) polished mount of pisolitic duricrust, showing cored ROIs and (U–Th)/He dates; b) radial plot of (U–Th)/He dates for the large pisolite in (a). Two age clusters are indicated, with the rim of the pisolite younger than the core. The distance (σ) along the radial projections for the rim and core gives a measure of the precision of (U–Th)/He dates, with more precise dates in red and less precise dates in yellow

The evolved He volumes measured for the rim are also less than that measured for the pisolite core (Appendix).

Discussion

The multiple characterization techniques employed in this study establish that the black pisolites in the pisolitic duricrusts are the most suitable sample media for (U–Th)/He dating. The pisolitic duricrust matrix and fragmental duricrust are deemed unsuitable for dating because of their complex textural and mineralogical inhomogeneity at the scale of sampling (i.e. mini-core drilling). However, careful sample selection (e.g. GSWA 226969 and 226970) did yield iron oxide-rich (lithic) fragments suitable for dating.

Despite the small number of samples in this study, the relative consistency of the analytical results for individual pisolites suggests that the (U–Th)/He dating method can provide quantitative constraints on the relative timing of duricrust formation associated with lateritization in the Darling Range. The generally older ages measured for pisolitic duricrust relative to the underlying fragmental duricrust (Table 5) is consistent with pisolite formation occurring locally elsewhere prior to formation of fragmental duricrust via the direct ‘gibbsitization’ of saprock (Anand and Butt, 2003). Measured age variations from core to rim of a pisolite in sample GSWA 226923 suggest that pisolites either form by gradual accretive growth of Fe-oxide minerals over millions of years, or that the pisolite core initially formed about 3.9 million years ago and was subsequently modified by postaccretionary processes, such as episodic ancient bushfires, that most seriously affected the parent–daughter relationship in the outermost pisolite rims. Previous studies (e.g. Mitchell and Reiners, 2003) have shown that the thermal effect of a passing bushfire can induce helium loss in apatite and zircon, such that (U–Th)/He ages in the outermost 3 cm of an igneous rock surface were completely or partially reset by high temperatures (350–650°C) induced by fire over intervals of 5 to 40 minutes. An examination of the mineralogy of a large pisolite in sample GSWA 226923 (Fig. 7) confirms a difference between the core (3.9 ± 0.5 Ma) and rim (2.0 ± 0.2 Ma), with the rim consisting of a mixture of maghemite, gibbsite, and hematite, whereas the core is mainly maghemite, gibbsite, and poorly crystalline alumina (PCA) phases (possibly the κ - and θ -polytypes) (Fig. 8).

The presence of hematite, maghemite, corundum, and PCA in Darling Range laterites, as identified in the current study, is consistent with earlier studies (e.g. Anand and Gilkes, 1987; Anand and Butt, 2003). The reported field relationships for this mineral association suggest that maghemite, corundum, and PCA may form via the dehydroxylation of Fe and Al oxyhydroxides, such as Al-substituted goethite, at temperatures between 300 and 500°C in the presence of organic matter during ancient periodic bushfires or directly via the transformation of Al-hydroxides, such as gibbsite (Anand and Gilkes, 1987;

Wells et al., 1989). Corundum formation likely occurs through a series of transitional (PCA) alumina phases (e.g. χ -, κ -, δ -, θ - or γ -types) with final crystallization of corundum at a higher temperature, in the range 900–1200°C.

Regardless of the precise mechanism of formation, the presence of maghemite, corundum, and PCA in the BGM lateritic duricrust suggests that the pisolite materials were thermally modified by bushfire events. The extent to which these bushfires have reset the (U–Th)/He ages is unknown and will be the subject of further enquiry.

Conclusions

Pisolites and pisolite nodules are suitable for (U–Th)/He dating due to their relative mineralogical and textural homogeneity, whereas the relatively complex mineralogy and high porosity of the duricrust matrix and cutans makes them unsuitable. Dates ranging from 5.7 to 1.3 Ma, measured on pisolitic and fragmental duricrust from exposed laterite profiles near the BGM, indicate late Miocene–Pliocene to possible early Pleistocene ages for duricrust formation and/or modification. These ages are comparable to the (U–Th)/He ages of Toodyay pisolites (Pidgeon et al., 2004), suggesting that processes of regolith formation and/or modification in the Darling Range were regionally synchronous.

This study shows that hematite–maghemite pisolites and nodules are suitable for (U–Th)/He dating and can provide quantitative age information on regolith formation processes. These dates can only be interpreted as formation ages if the pisolite-bearing material was buried more than several centimetres below the surface during a bushfire event. The presence of maghemite, corundum, and poorly crystalline alumina in the pisolites may indicate syn- or postformation modification by bushfire events, and the potential for total or partial resetting of (U–Th)/He ages. The effect of bushfires on (U–Th)/He ages of Fe-oxide minerals needs to be systematically investigated before the technique can be applied with confidence. However, the isotopic technique remains useful in providing quantitative constraints on the minimum age of regolith formation.

Acknowledgements

Thanks to Graeme Reynolds of Newmont for providing access to BGM. The assistance of Kelly Merigot and Veronica Avery in sample preparation and data collection is greatly appreciated. Thomas Bekker is thanked for his assistance with the Raman spectroscopic analysis. The TIMA instrument used in this study is part of the ARC Digital Mineralogy Hub Facility funded by ARC LE140100150. Funding for the project was provided by the Geological Survey of Western Australia (GSWA). Martin Danišák acknowledges the support of a Curtin Senior Research Fellowship.

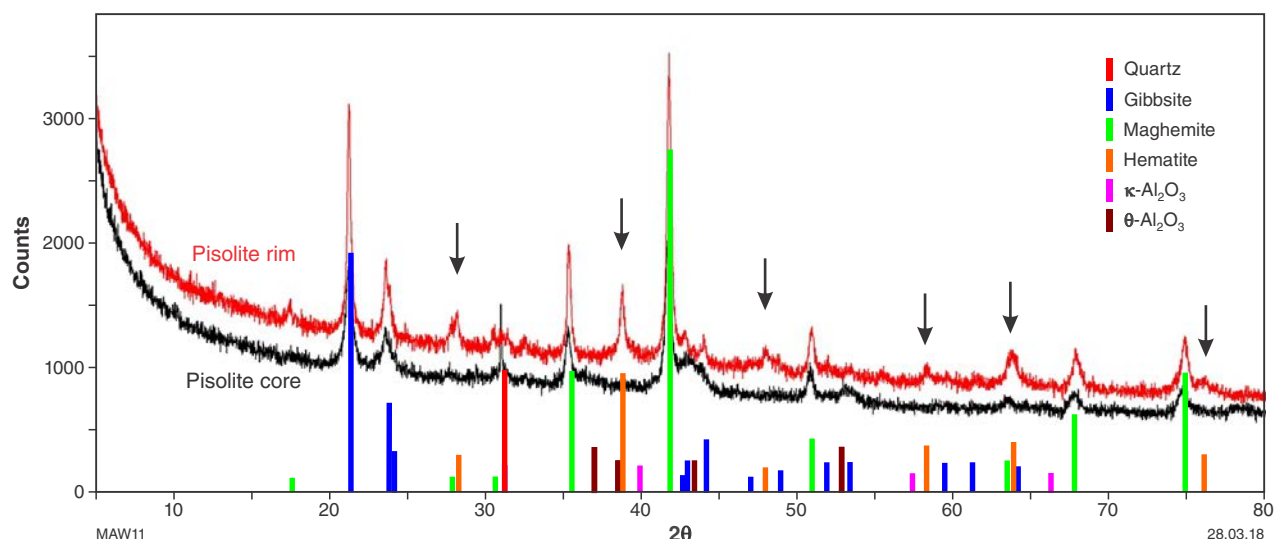


Figure 8. X-ray diffraction (XRD) patterns of the >300 micron size fractions for the pisolite rim and core in GSWA 226923 (Fig. 7). The rim is a mixture of maghemite, gibbsite, and hematite, whereas the core comprises maghemite, gibbsite, and poorly crystalline alumina phases (+ trace quartz and possibly hematite). The position of the main hematite diffraction peaks are arrowed

References

- Anand, RR 2005, Boddington gold deposit, Western Australia: CRC LEME Open file report, 3p.
- Anand, RR and Butt, CRM 2003, Distribution and evolution of 'Laterites' and lateritic weathering profiles, Darling Range, Western Australia: Australian Geomechanics – The Engineering Geology of Perth, Part 2, v. 38, no. 4, p. 41–58.
- Anand, RR and Gilkes, RJ 1987, The association of maghemite and corundum in Darling Range laterites, Western Australia: Australian Journal of Soil Research, v. 38, p. 607–622.
- Danišfk, M, Ramanaidou, ER, Evans, NJ, McDonald, BJ, Mayers, C and McInnes, BIA 2013, (U–Th)/He chronology of the Robe River channel iron deposits, Hamersley Province, Western Australia: Chemical Geology, v. 354, p. 150–162.
- Fanale, FP and Kulp, JL 1962, The helium method and the age of the Cornwall, Pennsylvania magnetite ore: Economic Geology, v. 57, p. 735–746.
- Heim, JA, Vasconcelos, PM, Shuster, DL, Farley, KA and Broadbent, G 2006, Dating paleochannel iron ore by (U–Th)/He analysis of supergene goethite, Hamersley province, Australia: Geology, v. 34, no. 3, p. 173–176.
- McCuaig, TC, Behn, M, Stein, H, Hagemann, SG, McNaughton, NJ, Cassidy, KF, Champion, D and Wyborn, L, 2001 The Boddington gold mine: A new style of Archaean Au–Cu deposit, in Cassidy, KF, Dunphy, JM and Van Kranendonk, MJ, 2001 4th International Archaean Symposium, Extended Abstracts AGSO/Geoscience Australia Record 2001/37, p. 453–455.
- Mitchell, SG and Reiners, PW 2003, Influence of wildfires on apatite and zircon (U–Th)/He ages: Geology, v. 31, no. 12, p. 1025–1028.
- Pidgeon, RT, Brander, T and Lippolt, HJ 2004, Late Miocene (U+Th)–4He ages of ferruginous nodules from lateritic duricrust, Darling Range, Western Australia: Australian Journal of Earth Sciences, v. 51, p. 901–909.
- Pillans, B 2005, Geochronology of the Australian regolith, in Regolith-landscape evolution across Australia edited by RR Anand and P de Broekert, CRC LEME Monograph, p. 41–61.
- Ramanaidou, ER, Wells, M, Lau, I and Laukamp, C 2015, Characterization of iron ore by visible and infrared reflectance and Raman spectroscopies, in Iron ore: mineralogy, processing and environmental issues edited by L Lu, Chapter 6, p. 191–228, Woodhead Publishing, Elsevier.
- Ruan, HD, Frost, RL and Klopogge, JT 2001, Comparison of Raman spectra in characterizing gibbsite, bayerite, diasporite and boehmite: Journal of Raman Spectroscopy, v. 32, p. 745–750.
- Vasconcelos, PM, Heim, JA, Farley, KA, Monteiro, H and Waltenberg, K 2013, Ar-40/Ar-39 and (U–Th)/He–He4/He-3 geochronology of landscape evolution and channel iron deposit genesis at Lynn Peak, Western Australia: Geochimica et Cosmochimica Acta, v. 117, p. 283–312.
- Vermeesch, P 2009, RadialPlotter: a Java application for fission track, luminescence and other radial plots: Radiation Measurements, v. 44, no. 4, p. 409–410.
- Wells, MA, Gilkes, RJ and Anand, RR 1989, The formation of corundum and aluminous hematite by the dehydroxylation of aluminous goethite: Clay Minerals, v. 24, p. 513–530.
- Wernicke, RS and Lippolt, HJ 1994, Dating of vein specularite using internal (U+Th)/He isochrons: Geophysical Research Letters, v. 21, no. 5, p. 345–347.

Appendix

Raw and corrected (U–Th)/He dates and measured U, Th and He concentrations for analysed duricrust samples

Sample code	^{232}Th (ng)	\pm (%)	^{238}U (ng)	\pm (%)	^{147}Sm (ng)	\pm (%)	He (ncc)	\pm (%)	TAU (%)	Th/U	Raw date (Ma) $\pm 1\sigma$ (Ma)	F_t	\pm (%)	Corrected He date (Ma) $\pm 1\sigma$ (Ma)
GSWA 226971														
971_R1A_roi2-1	0.202	2.6	0.021	3.0	0.002	28.4	0.055	3.9	4.4	9.55	6.6	1.00	10	6.6 0.7
971_R1A_roi2-2	0.150	1.7	0.014	2.2	0.001	41.3	0.035	5.9	6.1	10.81	5.8	1.00	10	5.8 0.7
971_R1A_roi2-3	0.104	1.8	0.010	2.4	0.003	28.7	0.026	7.8	8.0	10.06	6.1	1.00	10	6.1 0.8
971_R1A_roi2-4	0.137	1.7	0.018	2.3	0.001	46.5	0.035	4.9	5.1	7.57	5.7	1.00	10	5.7 0.6
971_R1A_roi2-5	0.285	2.4	0.028	2.8	0.002	27.9	0.052	3.9	4.4	10.24	4.6	1.00	10	4.6 0.5
971_R1A_roi3-1	0.091	2.5	0.019	2.8	0.003	32.7	0.025	7.2	7.5	4.82	5.2	1.00	10	5.2 0.7
971_R1A_roi3-2	0.095	1.8	0.020	2.4	0.005	23.1	0.017	9.9	10.0	4.62	3.3	1.00	10	3.3 0.5
971_R1A_roi3-3	0.074	1.8	0.016	2.3	0.003	31.6	0.019	9.6	9.8	4.57	4.6	1.00	10	4.6 0.6
971_R1A_roi3-4	0.063	1.8	0.011	2.2	0.002	33.4	0.009	18.2	18.3	5.68	2.9	1.00	10	2.9 0.6
971_R1A_roi3-5	0.140	2.5	0.028	2.9	0.004	25.0	0.024	6.2	6.5	4.91	3.2	1.00	10	3.2 0.4
971_R1B_roi4-1	0.127	2.5	0.014	2.8	0.001	57.0	0.027	6.1	6.4	8.87	5.0	1.00	10	5.0 0.6
971_R1B_roi4-2	0.096	1.8	0.013	2.6	0.001	27.7	0.031	4.5	4.7	7.07	7.1	1.00	10	7.1 0.8
971_R1B_roi4-3	0.233	1.7	0.034	2.2	0.001	27.4	0.057	3.8	4.1	6.88	5.3	1.00	10	5.3 0.6
971_R1B_roi4-4	0.107	1.8	0.015	2.4	0.002	25.0	0.035	5.0	5.2	6.94	7.1	1.00	10	7.1 0.8
971_R1B_roi4-5	0.065	2.4	0.009	2.8	0.002	29.0	0.013	11.4	11.5	6.99	4.4	1.00	10	4.4 0.7
971_R1B_roi5-1	0.087	1.8	0.015	2.3	0.002	17.5	0.015	10.1	10.2	5.88	3.5	1.00	10	3.5 0.5
971_R1B_roi5-2	0.152	1.7	0.019	2.2	0.001	25.8	0.025	6.3	6.5	8.11	3.8	1.00	10	3.8 0.4
971_R1B_roi5-3	0.142	1.7	0.012	2.3	0.001	29.0	0.017	9.0	9.1	11.58	3.1	1.00	10	3.1 0.4

Sample code	^{232}Th (ng)	\pm (%)	^{238}U (ng)	\pm (%)	^{147}Sm (ng)	\pm (%)	He (ncc)	\pm (%)	TAU (%)	Th/U	Raw date (Ma) $\pm 1\sigma$ (Ma)	Ft	\pm (%)	Corrected He date (Ma) $\pm 1\sigma$ (Ma)	
971_R1B_roi5-4	0.052	1.8	0.009	2.2	0.002	39.2	0.013	12.4	12.5	5.73	5.1	1.00	10	5.1	0.8
971_R1B_roi5-5	0.149	1.7	0.016	2.4	0.002	26.8	0.021	8.5	8.6	9.36	3.4	1.00	10	3.4	0.4
GSWA 226965															
965_R2_roi2-1	0.291	1.7	0.019	2.5	0.003	39.8	0.076	8.0	8.1	14.86	7.1	1.00	10	7.1	0.9
965_R2_roi2-2	1.993	1.7	0.173	2.4	0.002	33.0	0.309	2.2	2.6	11.42	3.9	1.00	10	3.9	0.4
965_R2_roi2-3	0.961	1.7	0.083	2.3	0.002	33.3	0.229	2.7	3.0	11.56	6.1	1.00	10	6.1	0.6
965_R2_roi2-4	1.182	1.7	0.120	2.2	0.003	25.4	0.244	2.3	2.7	9.74	5.0	1.00	10	5.0	0.5
965_R2_roi2-5	1.061	1.7	0.056	2.3	0.003	27.7	0.148	3.5	3.8	18.90	4.0	1.00	10	4.0	0.4
965_R2_roi3-1	0.432	1.7	0.032	2.3	0.003	32.2	0.055	9.6	9.7	13.30	3.4	1.00	10	3.4	0.5
965_R2_roi3-2	0.757	1.7	0.048	2.5	0.001	27.7	0.086	4.8	5.0	15.73	3.1	1.00	10	3.1	0.4
965_R2_roi3-3	0.967	1.7	0.100	2.3	0.001	41.3	0.106	3.6	3.8	9.58	2.7	1.00	10	2.7	0.3
965_R2_roi3-4	0.579	1.7	0.039	2.3	0.002	35.9	0.059	6.0	6.1	14.75	2.8	1.00	10	2.8	0.3
965_R2_roi3-5	0.657	1.7	0.060	2.5	0.001	49.4	0.107	3.4	3.7	10.90	4.1	1.00	10	4.1	0.4

Sample code	^{232}Th (ng)	\pm (%)	^{238}U (ng)	\pm (%)	^{147}Sm (ng)	\pm (%)	He (ncc)	\pm (%)	TAU (%)	Th/U	Raw date (Ma) $\pm 1\sigma$ (Ma)	F_t	\pm (%)	Corrected He date (Ma) $\pm 1\sigma$ (Ma)	
923_R3_roi4-1 rim	0.428	1.7	0.029	2.1	0.003	39.1	0.027	7.6	7.7	14.41	1.7	1.00	10	1.7	0.2
923_R3_roi4-1 rim	0.375	1.7	0.024	2.3	0.002	46.9	0.034	5.5	5.7	15.53	2.5	1.00	10	2.5	0.3
923_R3_roi4-1 rim	2.019	2.5	0.459	2.8	0.009	4.0	0.037	7.4	7.7	4.36	0.3	1.00	10	0.32*	0.04*
923_R3_roi4-1 core	0.233	2.4	0.030	2.8	0.005	20.0	0.029	11.5	11.6	7.75	2.8	1.00	10	2.8	0.4
923_R3_roi4-1 core	0.523	1.7	0.061	2.2	0.001	24.4	0.080	5.5	5.7	8.48	3.6	1.00	10	3.6	0.4
923_R3_roi4-1 core	0.452	1.7	0.052	2.1	0.002	29.1	0.080	6.6	6.8	8.56	4.1	1.00	10	4.1	0.5
923_R3_roi4-1 core	0.246	1.7	0.030	2.1	0.002	35.1	0.037	14.1	14.2	8.22	3.5	1.00	10	3.5	0.6
923_R3_roi4-1 core	0.490	2.5	0.051	2.8	0.002	40.8	0.099	6.7	7.0	9.49	4.9	1.00	10	4.9	0.6
GSWA 226969															
969_R1B_roi1-1	0.170	1.7	0.076	2.5	0.002	20.1	0.039	25.1	25.2	2.24	2.8	1.00	10	2.8	0.8
969_R1B_roi1-2	0.269	1.7	0.042	2.2	0.002	30.3	0.039	25.3	25.3	6.41	3.1	1.00	10	3.1	0.8
969_R1B_roi1-3	0.175	1.7	0.173	2.3	0.003	25.4	0.074	9.6	9.8	1.00	2.8	1.00	10	2.8	0.4
969_R1B_roi1-4	0.209	2.4	0.079	2.7	0.003	18.7	0.043	26.1	26.2	2.63	2.8	1.00	10	2.8	0.8
969_R1B_roi1-5	0.100	1.8	0.055	2.3	0.002	26.2	0.031	28.6	28.6	1.80	3.2	1.00	10	3.2	1.0
GSWA 226970															
970_MottleDat-1	27.124	1.7	0.055	2.2	0.000	11.5	1.022	3.3	3.7	490.74	1.3	1.00	10	1.3	0.1
970_MottleDat-2	59.289	1.7	0.117	2.3	0.002	38.6	2.232	3.2	3.6	503.22	1.3	1.00	10	1.3	0.1
970_MottleDat-3	84.239	2.6	0.166	2.9	0.002	33.4	3.698	3.2	4.1	504.71	1.5	1.00	10	1.5	0.2
970_MottleDat-4	54.510	1.7	0.171	2.5	0.001	34.2	1.421	3.2	3.6	316.40	0.9	1.00	10	0.9	0.1
970_MottleDat-5	85.257	1.7	0.198	2.6	0.001	53.4	3.437	3.2	3.6	426.68	1.4	1.00	10	1.4	0.1

NOTES: *The corrected He date (0.32 Ma) for sample '923_R3_roi4-1 rim' is an outlier and is not included in subsequent data analysis. Abbreviations: ncc, nano cubic centimetres; TAU, the Total Analytical Uncertainty (1 sigma in %); Ft, the Alpha Ejection Correction Factor (1 \pm 10%), and is the same for all samples

This Record is published in digital format (PDF) and is available as a free download from the DMIRS website at
<www.dmp.wa.gov.au/GSWApublications>.

Further details of geological products produced by the Geological Survey of Western Australia can be obtained by contacting:

Information Centre
Department of Mines, Industry Regulation and Safety
100 Plain Street
EAST PERTH WESTERN AUSTRALIA 6004
Phone: +61 8 9222 3459 Fax: +61 8 9222 3444
www.dmp.wa.gov.au/GSWApublications

(U-TH)/HE DATING OF FERRUGINOUS DURICRUST,
BODDINGTON GOLD MINE, WESTERN AUSTRALIA

